A New Method for Quantitative Marking of Deposited Lithium via Chemical Treatment on Graphite Anodes in Lithium-Ion Cells

Yvonne Krämer*[a], Claudia Birkenmaier[b], Julian Feinauer[a,c], Andreas Hintennach[b], Conrad L. Bender[d], Markus Meiler[a], Volker Schmidt[c], Robert E. Dinnebier*[e] and Thomas Schleid[f]

Abstract: A novel approach for the marking of deposited lithium on graphite anodes from large automotive lithium-ion cells (≥ 6 Ah) is presented. Graphite anode samples were extracted from two different formats (cylindrical and pouch cells) of pristine and differently aged lithium-ion cells. The samples present a variety of anodes with various states of lithium deposition (also known as plating). A chemical modification was performed to metallic lithium deposited on the anode surface due to previous plating with isopropanol (IPA). After this procedure an oxygenated species was detected by scanning electron microscopy (SEM), which later was confirmed as Li_2CO_3 via Fourier transform infrared spectroscopy (FT-IR) and X-ray powder diffraction (XRPD). A valuation of the covered area by Li_2CO_3 was carried out with an image analysis using energy dispersive X-ray spectroscopy (EDX) and quantitative Rietveld refinement.

The majority of lithium-ion cells contains a graphite-based anode for intercalation and deintercalation (0.05 – 0.30 V vs- Li^+/Li) of Li^+ during charging or discharging.[1,2] Normally, lithium-ion cells do not contain metallic lithium. Graphite anodes operate at a potential outside of the electrochemical stability window of the electrolyte components.[3] Therefore, changes on the electrode-to-electrolyte interface due to the electrolyte decomposition accompanied by irreversible consumption of lithium ions occur when the electrode is in a charged state.[4] A solid electrolyte interface (SEI) is formed which is permeable for Li^+ but prevents electron transfer[5,6]. If the anode potential drops below 0 V vs. Li^+/Li, metallic lithium (plating) can precipitate on the anode surface due to the combination of charging at low temperatures, high state-of-charge (SOC) and high charge rates.[7,8] Also the size and shape of a cell affects the behaviour of lithium deposition. Due to longer distances inside an automotive cell diffusion rates can vary more than in small consumer or lab cells. This also results in inhomogeneous electric fields which can affect the process of lithium deposition. Long-term effects of lithium deposition are capacity loss, decrease in Coulomb efficiency and rise of impedance. Prediction of lithium deposition during various conditions in large lithium-ion cells cannot be done from data of small lab cells.

In this study we demonstrate a novel chemical treatment procedure via IPA at different types of large automotive lithium-ion cells. As mentioned before the size and format affects the formation of lithium deposition. As known to the authors, no other work has published before where lithium deposition in such cells has been investigated. Given this situation in this work we report a new method for qualitative and quantitative marking of deposited metallic lithium in large lithium-ion cells via chemical treatment with IPA to obtain zabuyelite (Li_2CO_3), which can be observed via high-resolution XRPD. Anode samples were cycled and extracted as described[9] from HEV (Hybrid Electric Vehicle) cylindrical (**A1**) and EV (Electric Vehicle) pouch cells (**A2**), separated, washed with DMC, IPA and dried at 25 °C in air (Figure 1a). On the same spots of deposited lithium on the surface of the anode the white coating of Li_2CO_3 was obtained after 10 min through oxidation of C_3H_7O-Li/OH-Li and CO_2 from air (Figure 1b and 1c).

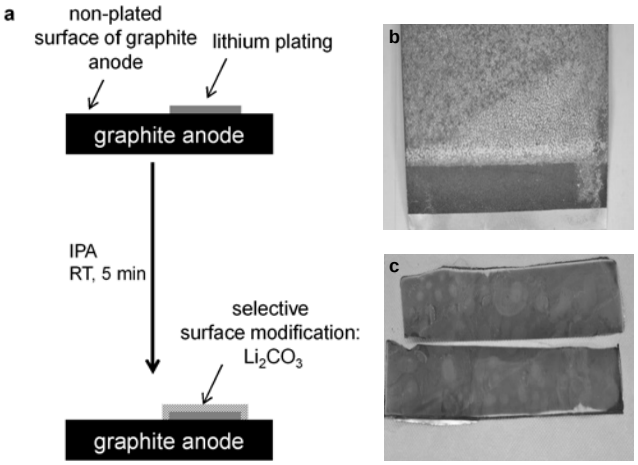

Figure 1. a) Surface modification process, b) anode **A1**, c) anode **A2**.

Initially, the composition of the white coating of A1 (58.78 %) and A2 (56.83 %) was investigated with SEM/EDX (1.3 mm x 1.6 mm, Figure 2). The colors in Figure 2 represent the oxygen (green) and carbon signal (red) distribution. Other EDX signals from P, F and Cu are not shown. The white coating exhibits a maximum height of 50 μm.

The Li_2CO_3 area itself has a stable, but brittle surface, where individually grown lit deposition dendrites were merged together

[a] Y. Krämer, J. Feinauer, Dr. M. Meiler
Deutsche ACCUmotive GmbH & Co. KG
Neue Straße, 95, 73230 Kirchheim unter Teck (Germany)
E-mail: yvonne.kraemer@daimler.com
Fax: +49 711 3052 127780
[b] C. Birkenmaier, Dr. Dr. A. Hintennach
Daimler AG
Mercedesstraße 143, 70546 Stuttgart (Germany)
[c] J. Feinauer, Prof. Dr. V. Schmidt
Institute of Stochastics, Ulm University
Helmholtzstraße 18, 89069 Ulm (Germany)
[d] C. L. Bender
Physikalisch-Chemisches Institut, Universität Gießen
Heinrich-Buff-Ring 58, 35392 Gießen (Germany)
[e] Prof. Dr. R. E. Dinnebier
Max Planck Institute for Solid State Research
Heisenbergstraße 1, 70569 Stuttgart (Germany)
E-Mail: r.dinnebier@fkf.mpg.de
Fax: +49 711 689 1502
[f] Prof. Dr. Th. Schleid
Institut für Anorganische Chemie, Universität Stuttgart
Pfaffenwaldring 55, 70569 Stuttgart (Germany)

during ageing. Spherical graphite particles (red) are visible on the right side of the image of **A2** (Figure 2b).
In the middle, first areas with Li_2CO_3 are visible, which continue to merge on the left side until a planar area is visible. Here the Li_2CO_3 part is thinner with a mossy texture.

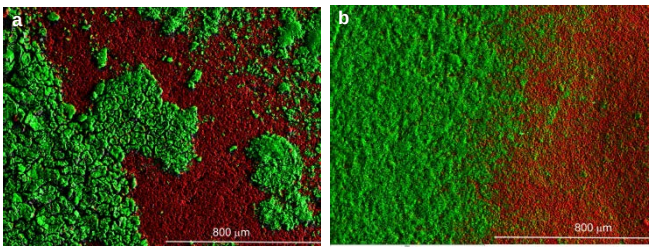

Figure 2. SEM/EDX images with oxygen (green) and carbon (red) signals of a) the anode sample **A1**, 58.78 % covered with Li_2CO_3; b) the anode sample **A2**, 56.83 % covered with Li_2CO_3 (see supporting information).

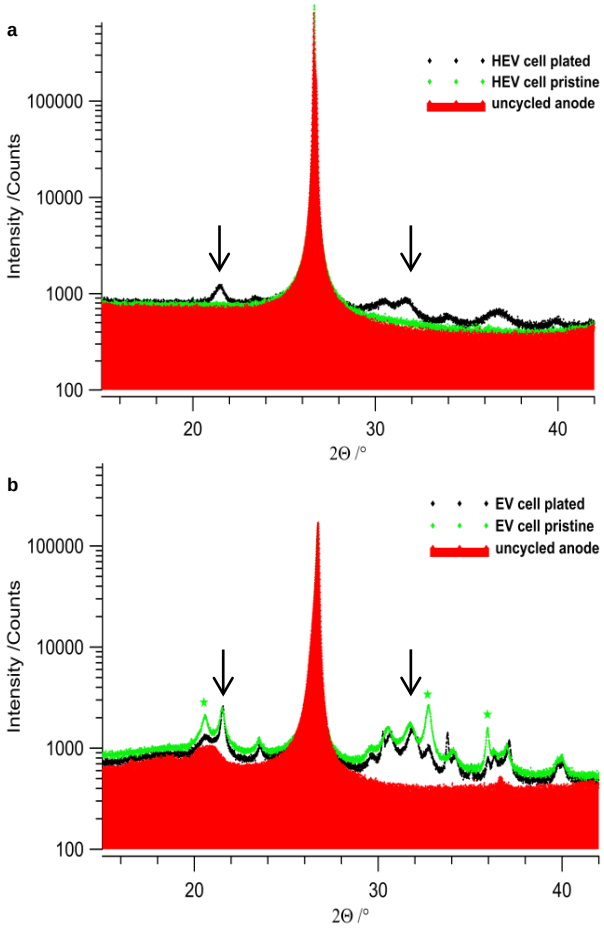

Figure 3. XRPD patterns in Bragg-Brentano geometry of *uncycled* (red), *pristine* (green) and *aged* (plated, black) a) anode sample **A1,** b) anode sample **A2**. The presence of additional Li_2CO_3 peaks is clearly visible (denoted by →). LiOH peaks (denoted by *) in pristine and **A2** samples from EV cells are visible too.

The fraction of surface area covered by Li_2CO_3 was calculated using simple methods from mathematical morphology and stereology[10] to 55.78 % (**A1**) and 55.08 % (**A2**). XRPD data was collected for uncycled (before formation, no SEI), pristine (after formation, with SEI) and aged anodes (plated) (Figure 3a and 3b) in Bragg-Brentano geometry. All samples were pretreated as described. The XRPD patterns of the uncycled and pristine anode show one dominant peak indicating 2H-graphite (Figure 3a). Additional minor peaks representing Li_2CO_3 are present in the powder pattern of the plated sample **A1**. Hence, the film on the surface can therefore be identified as Li_2CO_3. Compared to previous work[9,11] we want to point out the safe chemical treatment with IPA to visualize lithium deposition performed on large automotive lithium ion cells and the precise verification of Li_2CO_3 via XRPD (denoted by arrow). This is the first time known to the authors that deposited metallic lithium on graphite anodes from large automotive cells can be conserved with the original frozen shape. As shown in the XRPD patterns of *pristine* graphite anodes from HEV and EV cells, this method is also sensitive for normal lithiated anodes and shows no Li_2CO_3 peaks; neither from deposited lithium nor the SEI.

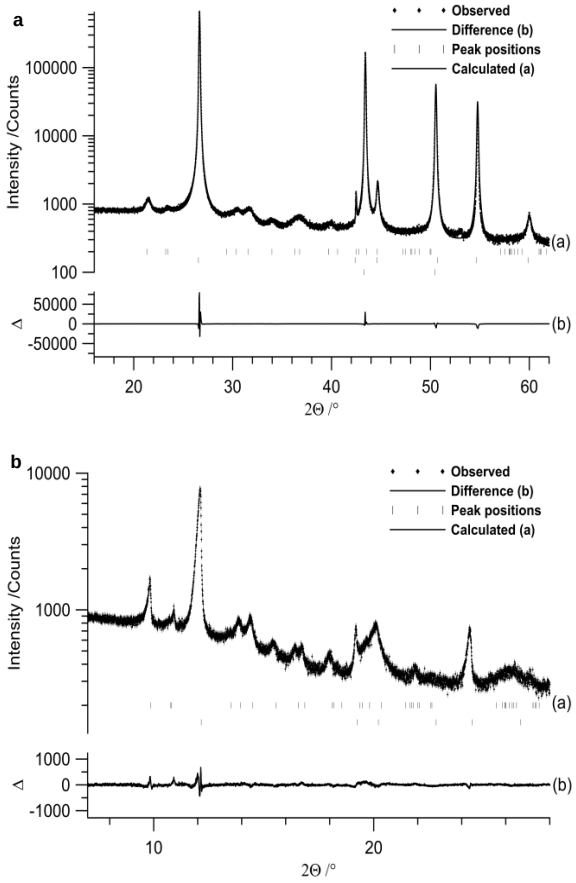

Figure 4. Section of the Rietveld plot of aged (plated) anodes measured in Debye-Scherrer geometry, a) anode from HEV sample **A1** (Li_2CO_3: 27 wt %, 2H-graphite: 73 wt %). b) anode from EV sample **A2** (Li_2CO_3 (20 wt %, 2H-graphite: 80 wt %).

The powder pattern of the uncycled anode shows one dominant peak of pure 2H-graphite as well (Figure 3b). The additional broad peak at 20 – 22° is associated to PVDF. The XRPD pattern of the pristine anode already shows small amounts of LiOH and Li_2CO_3 at 20 – 22° which are formed as part of the solid electrolyte interface (SEI)[5,6]. The powder pattern of the plated sample **A2** also shows Li_2CO_3 and a lesser amount of LiOH. Metallic lithium reacts with IPA to form a layer on the SEI and coats the surface with LiOH. Compared to the pristine anode Li_2CO_3 from deposited lithium on the sample **A1** can also be conserved with IPA. For both samples **A1** and **A2** no Li_2CO_3 from the SEI was observed on the pristine graphite anode. To quantitatively determine the amount of Li_2CO_3, XRPD patterns of the anode active materials were collected in Debye-Scherrer geometry and analyzed via Rietveld refinement for samples **A1** (Figure 4a) and **A2** (Figure 4b). Small amounts of copper from sample preparation were detected for **A1**. The renormalized wt % of Li_2CO_3 and 2H-graphite are 27 wt % and 73 wt % for **A1** and 20 wt % and 80 wt % for **A2**. To confirm the formation of Li_2CO_3 additionally time-dependent FT-IR measurements were performed on sample **A2** in an argon-filled glove box. After pretreatment, the anode surface was wetted with IPA and dried in vacuum. FT-IR spectra were recorded after 10 min (Figure 5a, 4000 – 550cm^{-1}).

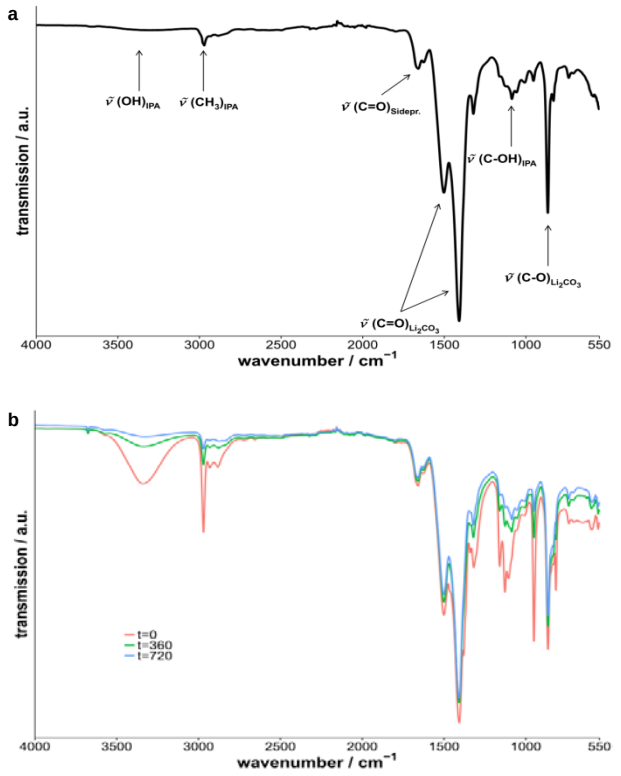

Figure 5. FT-IR measurement of IPA treated anode sample **A2** a) taken after t = 300 s and b) time-dependent taken after t = 0, 360 and 720 s.

Both dominant peaks in the ranges at 1500 cm^{-1} and at 900 cm^{-1} can be clearly identified as the characteristic peaks of Li_2CO_3. Both signals are due to $\tilde{\nu}$(C=O) and $\tilde{\nu}$(C–O) vibrations, respectively.[12] The residual IPA can be assigned to the broad signal at 3350 cm^{-1}, as well as to 2970 cm^{-1} and 1100 cm^{-1}, resulting from the -OH, -CH_3, and C=O-stretching of the molecule.[13,14] Formation of by-products during the oxidation process is indicated by the peak at 1700 cm^{-1}, which may arise from the carbonyl functional group of such a fragment. To prove the stability of Li_2CO_3, time-dependent IR measurements were conducted. The anode was treated as described. Surface IR spectra were taken in a glove box every 90 s. The results are given in Figure 5b for three exemplary time steps t = 0, 360 and 720 s. Despite the fact that IPA evaporation leads to decreased transmission intensities in relation to time (1200 cm^{-1} – 1000 cm^{-1}), all spectra show the same characteristics. Thus, neither a new peak is formed, nor an existing peak disappears. The product formed on **A2** is stable on surfaces.

Li_2CO_3 as part of the SEI was formerly observable in the XRPD pattern of the pristine anode from EV cell. With XRPD patterns it is impossible to decide, whether the Li_2CO_3 peaks arise from the SEI or from transformed metallic lithium. Simultaneously, the LiOH peaks in the XRPD pattern of **A2** increase from pristine to aged state, so we hypothesize that these peaks arise from a metallic lithium layer, which only reacted to LiOH with IPA and was then covered with an additional thin layer of Li_2CO_3 (Figure 6).

This theory is in agreement with the XRPD measurement in Debye-Scherrer geometry, where no more LiOH was observed. Moreover, no Li_2CO_3 from the SEI was detected in the XRPD patterns of HEV pristine anode. Accordingly, we conclude that the peaks concerning Li_2CO_3 in the XRPD pattern of **A1** are associated with the product of the chemical reaction of deposited lithium and IPA. For more information, see supporting information.

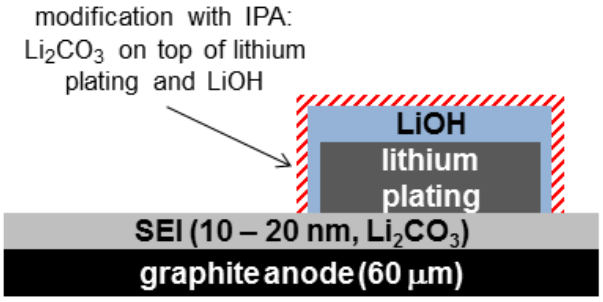

Figure 6. Schematic illustration (not true to scale) of the formation of LiOH and the following overlay with Li_2CO_3 after lithium deposition on the SEI.[15,16]

Experimental Section

Electrical tests were carried out until the cut-off voltage in respect to the used cathode-chemistry. For more information, see supporting information). The samples were extracted from cylindrical and pouch cells as described[9] at SOC = 0 %. All samples were washed with $C_3H_6O_3$ (DMC for synthesis, Merck KGaA). Chemical treatment was performed with C_3H_7OH (IPA, analytical grade, Merck KGaA). The samples were dried at 25 °C. SEM and EDX data was collected at CamScan CS44 (0.5 – 40 kV; (BSD-Robinson detector, INCA Energy 200 system with Si(Li) detector, resolution ± 1 µm). HR-XRPD data was collected on laboratory powder diffractometers. Anode plates of square shape (20 mm^2) were placed as is on silicon wafers with circular cavities.

As diffractometer, a Bruker D8-Advance (Cu-$K_{\alpha1}$ radiation) in Bragg-Brentano geometry using a Lynx-Eye position-sensitive detector. Data was recorded in steps of 0.007° 2θ from 2.0 – 62.0° 2θ for 6 h. The powder patterns exhibited extreme preferred orientation. For quantitative analysis the graphite was scratched from the copper substrate and filled in 0.5 mm Hilgenberg borosilicate glass capillaries. As diffractometer, a Stoe-Stadi-P (Cu-$K_{\alpha1}$ radiation) and a Mythen-Dectris position-sensitive detector was used. Data was recorded in steps of 0.012° 2θ from 5.0 – 65.0° 2θ for 12 h. For quantitative Rietveld refinement[17] of the Debye-Scherrer data, the program TOPAS 5[18] was used. The peak profile and precise lattice parameters were determined by Pawley fits[19] using the fundamental parameter (FP) approach of TOPAS[20]. For modeling the background, Chebychev polynomials were employed. Starting values for the crystal structures of 2H-graphite[21], 3R-graphite[22], zabuyelite (Li_2CO_3)[23], LiOH[24] and copper[25] were taken from the ICSD database. ATR-FT-IR spectra were recorded with a Thermo Scientific Nicolet IS5 spectrometer (DTGS KBr detector, 4 cm^{-1} resolution, 32 scans).

Acknowledgements

This work was financially supported by the German BMBF under the grant number 03X4631. We thank Prof. Dr. Jürgen Janek from the Justus Liebig University in Giessen for FT-IR measurements, Tim Mitsch for electrical tests, Dr. Ralph Fischer and Christine Hiller for collecting SEM/EDX images.

Keywords: Lithium-Ion Battery • Lithium deposition • X-ray powder diffraction • Chemical treatment • Infrared spectroscopy

[1] O. Dolotko, A. Senyshyn, M. J. Mühlbauer, K. Nikolowski, H. Ehrenberg, *J. Power Sources* **2014**, *255*, 197–203.

[2] S. Tippmann, D. Walper, L. Balboa, B. Spier, W. G. Bessler, *J. Power Sources* **2014**, *252*, 305–316.

[3] K. Xu, *Chem. Rev.* **2004**, *104*, 4303–4417.

[4] J. Vetter, P. Novák, M. R. Wagner, C. Veit, K.-C. Möller, J. O. Besenhard, M. Winter, M. Wohlfahrt-Mehrens, C. Vogler, A. Hammouche, *J. Power Sources* **2005**, *147*, 269–281.

[5] E. Peled, D. Golodnitsky, G. Ardel, *J. Electrochem. Soc.* **1997**, *144*, 208–210.

[6] D. Aurbach, B. Markovsky, G. Salitra, E. Markevich, Y. Talyossef, M. Koltypin, L. Nazar, B. Ellis, D. Kovacheva, *J. Power Sources* **2007**, *165*, 491–499.

[7] N. Legrand, B. Knosp, P. Desprez, F. Lapicque, S. Raël, *J. Power Sources* **2014**, *245*, 208–216.

[8] W. Lu, C. M. López, N. Liu, J. T. Vaughey, A. Jansen, D. W. Dees, *J. Electrochem. Soc.* **2012**, *159*, 566–570.

[9] T. Mitsch, Y. Krämer, J. Feinauer, G. Gaiselmann, H. Markötter, I. Manke, A. Hintennach, V. Schmidt, *Materials (Basel).* **2014**, *7*, 4455–4472.

[10] S. N. Chiu, D. Stoyan, W. S. Kendall, J. Mecke, *Stochastic Geometry and Its Applications*, John Wiley & Sons, Chichester, **2013**.

[11] M. Zier, F. Scheiba, S. Oswald, J. Thomas, D. Goers, T. Scherer, M. Klose, H. Ehrenberg, J. Eckert, *J. Power Sources* **2014**, *266*, 198–207.

[12] D. Aurbach, E. Yair, A. Zaban, *Electrochem. Soc. Lett.* **1994**, *141*, 9–11.

[13] E. Pretsch, P. Bühlmann, M. Badertscher, *Spektroskopische Daten Zur Strukturaufklärung Organischer Verbindungen*, Springer, Berlin Heidelberg, **2010**.

[14] C. Barakat, P. Gravejat, O. Guaitella, F. Thevenet, A. Rousseau, *Appl. Catal. B Environ.* **2014**, *147*, 302–313.

[15] H. J. Ploehn, P. Ramadass, R. E. White, *J. Electrochem. Soc.* **2004**, *151*, A456–A462.

[16] E. Peled, *J. Electrochem. Soc.* **1979**, 2047–2051.

[17] H. M. Rietveld, *J. Appl. Crystallogr.* **1969**, *2*, 65–71.

[18] Bruker AXS, **2012**.

[19] G. S. Pawley, *J. Appl. Crystallogr.* **1981**, *14*, 357–361.

[20] R. W. Cheary, A. A. Coelho, J. P. Cline, *J. Res. Natl. Inst. Stand. Technol.* **2005**, *109*, 1–25.

[21] U. Hofmann, D. Wilm, *Proc. R. Soc. London, Ser. A Math. Phys. Sci.* **1936**, *155*, 345 – 365.

[22] H. Lipson, A. R. Stokes, *Proc. R. Soc. London, Ser. A Math. Phys. Sci.* **1942**, *181*, 101–105.

[23] Y.-Y. Lin, H.-Q. Zheng, *Chinese Sci. Bull.* **1990**, *35*, 489–490.

[24] S. L. Mair, *Acta Crystallogr. A* **1978**, *34*, 542–547.

[25] H. E. Swanson, E. Tatge, *Philos. Mag.* **1933**, *15*, 472–487.